Microchimica Acta (2020) 187:605
https://doi.org/10.1007/s00604-020-04575-2

ORIGINAL PAPER

Synthesis of dopamine-derived N-doped carbon nanotubes/Fe_3O_4 composites as enhanced electrochemical sensing platforms for hydrogen peroxide detection

Yanan Zhao[1,2] · Danqun Huo[1] · Liuyi Jiang[1] · Shiying Zhou[1] · Mei Yang[1] · Changjun Hou[1,3]

Received: 4 May 2020 / Accepted: 26 September 2020

Abstract

A novel preparation of dopamine-derived N-doped carbon nanotubes/Fe_3O_4 composites (N-CNTs/Fe_3O_4 Cs) is demonstrated via facile hydrothermal route and calcination treatment. In this approach, dopamine was selected as N-containing precursor, which can promote Fe_3O_4 nanocrystal deposition uniformly on the surface of CNTs and effectively modulated the graphitic structure with doped pyridinic N and graphitic N to improve the electrochemical performance of carbon composites. More interestingly, the inhibited growth of the Fe_3O_4 crystal during calcination can be effectively avoided by soaking PDA-CNT/Fe_3O_4 Cs in a phosphate solution before calcination. The N-CNTs/Fe_3O_4 Cs have an enhanced electrocatalytic activity toward hydrogen peroxide with high sensitivity (316.27 mA M^{-1} cm^{-2}) and wide linear range (0.006–2.057 mM). The N-CNTs/Fe_3O_4 Cs modified sensor was successfully applied to real-time detection of H_2O_2 released from living cancer cells, displaying a potential application in the study of oxidative stress-related diseases. This work demonstrates a rational way for high-performance electrocatalytic material synthesis and bioanalysis.

Keywords Polydopamine · N-doped carbon nanotubes · Fe_3O_4 · Hydrogen peroxide detection · Cancer cell H_2O_2 release

Introduction

Carbon composite is of growing interest for fabrication of excellent performance materials in sensoring devices, energy, and catalytic applications [1–3]. Owing to inherently inert of graphitic carbons, nanotubes (CNTs) generally require to be activated by chemical oxidation such as HNO_3 and H_2SO_4 [4] or developed the noncovalent interaction of biomolecules or polymers [5–7] to separate CNT agglomerates and facilitate the binding sites. Unfortunately, such oxygen-containing functionalization and molecules layers accompany defect formation that deteriorates the electrical properties and reduces electrical contact of composite with electrode interface [8, 9]. As an alternative functionalization method, heteroatom-doping has been in focus of CNT research in the recent years [10]. Electro-rich nitrogen (N)/sulfur (S)/phosphor (P)-doped CNT integrated with other functional components may work synergistically for performance optimization. Meanwhile, during doping process, the graphitic surface of CNTs can be effective functionalization by means of functional groups such as hydroxyl or carboxyl that act as anchoring sites to deposit

Electronic supplementary material The online version of this article (https://doi.org/10.1007/s00604-020-04575-2) contains supplementary material, which is available to authorized users.

✉ Danqun Huo
huodq@cqu.edu.cn

✉ Mei Yang
yangmei@cqu.edu.cn

✉ Changjun Hou
houcj@cqu.edu.cn

[1] Key Laboratory for Biorheological Science and Technology of Ministry of Education, State and Local Joint Engineering Laboratory for Vascular Implants, Bioengineering College, Chongqing University, Chongqing 400044, People's Republic of China

[2] Analytical and Testing Center of Southwest University, Chongqing 400715, People's Republic of China

[3] Chongqing Key Laboratory of Bio-perception & Intelligent Information Processing, School of Microelectronics and Communication Engineering, Chongqing University, Chongqing 400044, People's Republic of China

Published online: 13 October 2020

metal–metal oxide nanocrystals, achieving the metal-containing heteroatom doped carbon composites.

Until now, the carbonization of precursor chemicals such as aniline, urea, and pyrrole has been accepted as an effective method for preparing N-doped carbon composite [11–13]. More importantly, N with excessive valence electrons that can be introduced into the graphene lattice could greatly improve limiting current density and the onset potential [14], achieving a high electrochemical performance for target reactions. Despite recent progress, the improved properties of N-containing precursors are necessary for maintaining electrical properties of CNTs as well as effective modulation of graphitic structure. Polydopamine (PDA) is a kind of biopolymer derived from a polymerization of dopamine in alkaline aqueous solutions, which is well-known for its excellent affinity to various substrates and nanostructures [15]. Studies show carbonized polydopamine (C-PDA) coatings have a multi-layered graphene-like structure and high electrical conductivity to that of N-doped graphene [16, 17]. Evidence also points out there is little sp^3 C in final PDA-based carbon matrix from the ^{13}C NMR spectra and XPS analysis [18]. Minimizing sp^3 C occurring in carbon structures can enhance the electroconductivity. In addition, many types of metal ions can chelate with catechol and amine groups of PDA [19–21], allowing facile modification of functional materials into the PDA-based N-doped carbon matrix for many applications.

With this point of view, dopamine-derived N-doped CNT/Fe_3O_4 composites (N-CNT/Fe_3O_4 Cs) were prepared via facile hydrothermal route coupled with a simple calcination treatment (Scheme 1). PDA-modified CNTs (PDA-CNTs) have a good dispersion, in which the unique molecular structure of PDA can promote Fe_3O_4 nanocrystals deposition with uniformly distributed on the surface of CNTs. Fe_3O_4 nanocrystals have peroxidase-like activity, which exhibits catalytic performance for hydrogen peroxide (H_2O_2) reduction. The increased pyridinic N and graphitic N in N-CNT/Fe_3O_4 Cs were further improved electrochemical performance of carbon composites. This facile and effective method will open up a new avenue for the development of high-performance electrocatalytic materials for biosensenor and catalytic applications. Electrochemical measurement results show that loading of Fe_3O_4 on this conducting N-doped carbon carrier delivers enhanced sensitivity and selectivity toward H_2O_2 detection. H_2O_2, as a signaling molecule, is one of the most stable species of ROS generated in the biological system, which is closely related to some diseases ranging from cancer to neurodegenerative diseases [22]. To demonstrate the analytical applicability of the N-CNTs/Fe_3O_4 Cs, real-time detection of H_2O_2 released from living cells was further evaluated. Such N-CNT/Fe_3O_4 Cs-based biosensor can be successfully used for in situ detection of H_2O_2 released by living tumor cells during the redox homeostasis disrupted by drug, which show significant potentially useful for us to understand the information of the intracellular environment in the tumor developing process.

Experimental section

All reagents and apparatus are detailed in the Electronic Supplementary Material (ESM).

Preparation of N-CNT/Fe_3O_4 Cs and its modified electrode

PDA was spontaneously coated on CNT surface via oxidative polymerization in alkaline aqueous solutions. CNTs were dispersed in 100 ml of Tris-HCl buffer solution (pH 8.5) with a concentration of 1 mg mL^{-1} under sonication for 30 min. Two hundred milligrams of DA was added into the homogeneous CNTs suspension at a concentration of 2 mg mL^{-1}, and mild stirred for 24 h at room temperature. The obtained PDA-modified CNTs were centrifuged at 10000 rpm for 10 min, washed with DI water several times, and freeze dried in vacuum environment.

The N-CNT/Fe_3O_4 hybrid was synthesized via in situ self-assembly using hydrothermal method. Briefly, appropriate amount of freeze-dried PDA-CNTs was dispersed in 30 mL DI water under sonication. 0.7095 g $FeCl_3{\cdot}6H_2O$ was added into the PDA-CNTs dispersion and ultrasonicated for 15 min. Then, 0.6616 g $NaHCO_3$ and 0.088 g of L-ascorbic acid were added into the suspension under vigorously stirring. Subsequently, the mixture was transferred to Teflon-lined autoclave (50 mL) and kept in an air-flow electric oven at 150 °C for 6 h. The suspension was centrifuged, washed three times with DI water, and freeze-dried to obtain PDA-CNTs/Fe_3O_4 Cs. To avoid aggregation and growth of the hybrid during carbonization under high-temperature environment, the obtain PDA-CNTs/Fe_3O_4 Cs was soaked in 0.1 M NaH_2PO_4 solution for 48 h. After that, the as-prepared product was collected and washed with deionized water. The dried PDA-CNTs/Fe_3O_4 Cs were then annealed at 800 °C for 1 h in a pure argon atmosphere. Then, N-CNT/Fe_3O_4 Cs were obtained. N-CNT/Fe_3O_4 Cs was ultrasonic dispersed in nafion solution (0.05%) for preparation of a 5 mg mL^{-1} suspensions, and 4 μL of the as-prepared solution was dropped on the surface of the clean glassy carbon electrode (GCE) and dried at room temperature.

Cell culture and real-time detection of H_2O_2 released from cells

Human esophageal carcinoma cells EC-109 were purchased from BeNa Culture collection (Beijing, China), and cultured in a humidified incubator with 95% air and 5% CO_2 at 37 °C. EC-109 cells were grown in RPMI 1640 medium (Gibco) supplemented with 10% of fetal bovine serum (FBS) (Solarbio, China) and 1% penicillin-streptomycin (P/S) (Solarbio, China). When the cells were incubated 90% of the culture plate area, the cells were collected by centrifugation, washed three times with PBS, and then resuspended into PBS solution to

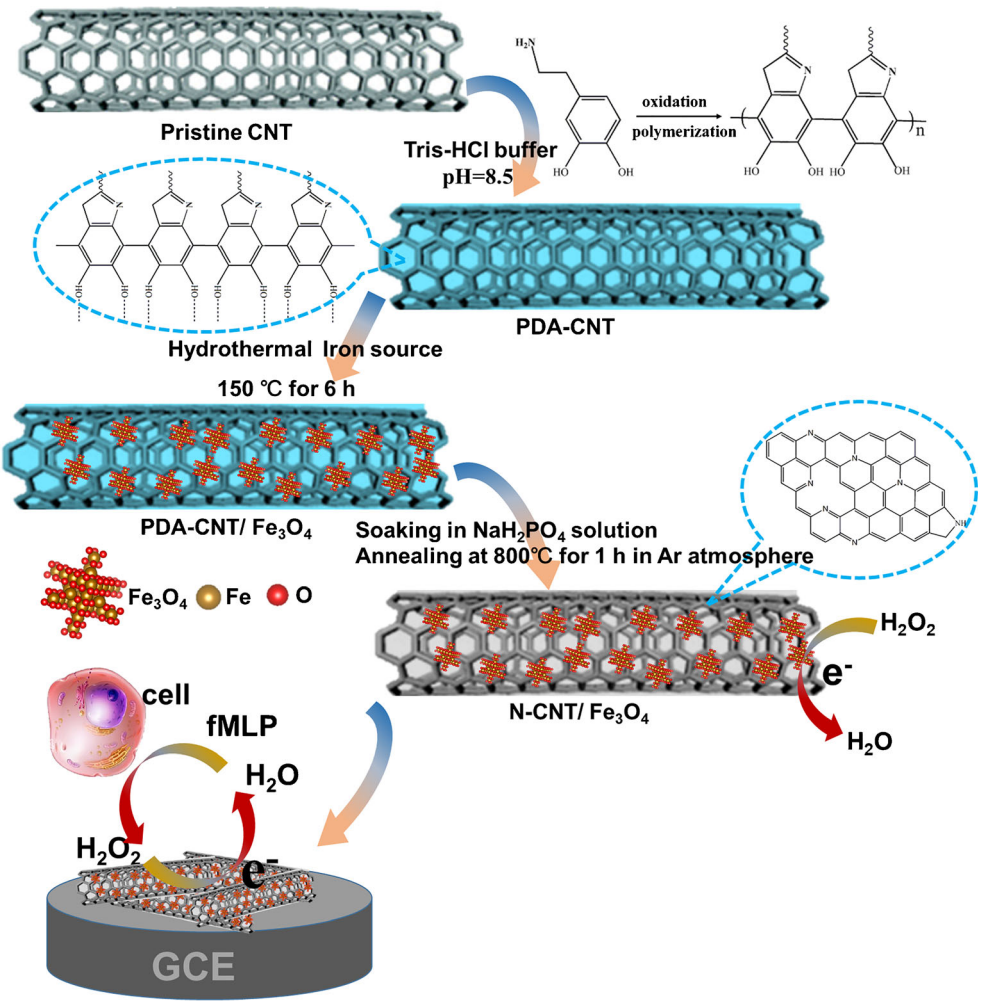

Scheme 1 Illustration of the nitrogen doping process for preparation of N-CNT/Fe_3O_4 and the modified GCE used for detecting H_2O_2 released from cells by stimulation of fMLP

count the number of cells (10^6 cells mL^{-1}) by a hemocytometer. Four micromolar fMLP as a model drug was injected into 2 mL of the as-prepared cell suspension, motivating cells generate H_2O_2 [23, 24]. As a control group, catalase was used as typical selective scavenger of H_2O_2 along with fMLP to investigate the specificity of the in situ monitoring of H_2O_2. Ten microliters of 200 μg mL^{-1} catalase was added to the cell suspension with fMLP at the same experimental condition. Amperometric current response of was recorded at applied potential of − 0.4 V based on the N-CNT/Fe_3O_4@GCE.

Results and discussion

Materials characterization

The dopamine was simultaneously oxidized and polymerized a thin surface coat on CNTs under alkaline conditions. As shown in Fig. 1a, the PDA-CNTs are curly shaped and randomly oriented, which still keep the original morphology of CNTs. It is noted in Fig. S1 that PDA modification on the surface of CNTs is ensured a good dispersion, which is further improved uniform distribution of the Fe_3O_4 nanocrystals on CNTs. The PDA-CNT/Fe_3O_4 Cs were synthesized by hydrothermal treatment, and it can be seen from Fig. 1b and Fig. S2 that Fe_3O_4 nanocrystals are adhered to the surface of CNTs. Unfortunately, the particles of Fe_3O_4 began to growth and crystallize into bulk material seriously during the annealing process (Fig. 1c and S2), which would affect the electrochemical performance of the as-prepared hybrids. The product was named bulk-N-CNT/Fe_3O_4 Cs. After PDA-CNT/Fe_3O_4 Cs soaked in 0.1 M phosphate solution and calcined at 800 °C for 2 h, it can be obviously seen that the morphology of as-prepared N-CNT/Fe_3O_4 Cs samples (Fig. 1d) was consistent with the morphology before calcination (Fig. 1b). It indicated that phosphate treatment played an important role in the inhibited growth of the crystal. The reason for that could be explained that phosphate ions deactivate the defect sites of Fe_3O_4 and prevent direct contact of particles because of the steric effect [25–27]. The EDS element analysis of N-CNT/Fe_3O_4 Cs also shows that synthesized sample is composed of C, O, N, and Fe elements (Fig. 1e).

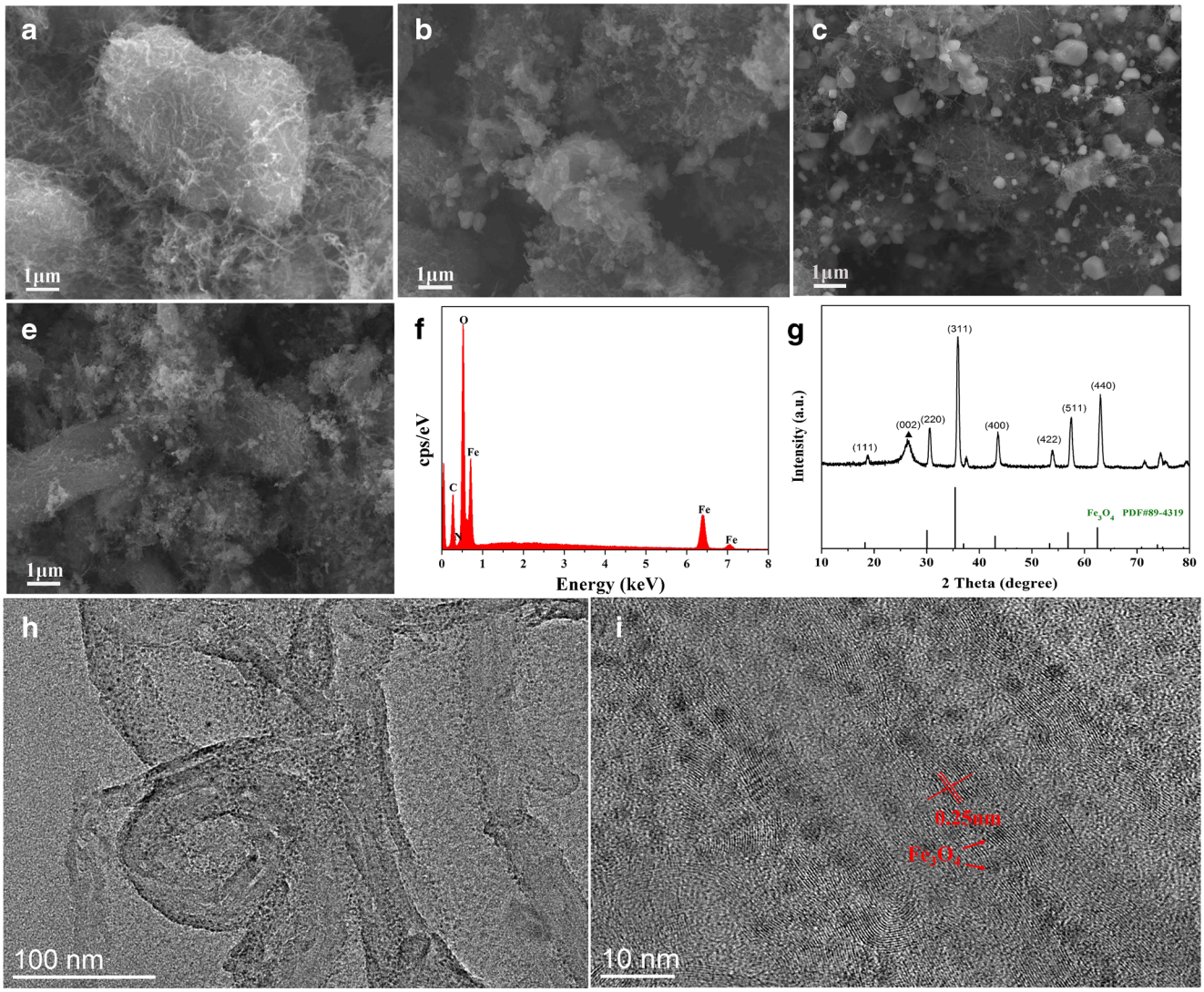

Fig. 1 FESEM images of PDA-CNTs (**a**), PDA-CNT/Fe_3O_4 (**b**), bulk-N-CNT/Fe_3O_4 (**c**), and N-CNT/Fe_3O_4 (**d**); EDS analysis (**e**); XRD patterns of as-prepared N-CNT/Fe_3O_4 (**f**) and TEM images of N-CNT/Fe_3O_4 (**g**, **h**)

The TEM images of N-CNT/Fe_3O_4 Cs in Fig. 1g exhibit that the ultrasmall Fe_3O_4 nanocrystals with an average size of 2.4 nm uniformly distributed on CNTs. The high-resolution TEM image of N-CNT/Fe_3O_4 Cs in Fig. 1h displays good crystal structure of the Fe_3O_4 nanocrystals with lattice distance about 0.25 nm, which is measured to correspond well to the (311) facets of the Fe_3O_4. From XRD patterns shown in Fig. 1f, the diffraction peaks of N-CNT/Fe_3O_4 Cs can be assigned to the cubic magnetite structure (JCPDS 89-4319), of which the peaks at approximately 35.8°correspond to the (311) planes of crystalline Fe_3O_4, coinciding well with the result of high-resolution TEM image. The diffraction peak at 26.2° is observed in sample corresponding to diffraction peak (002) of CNTs. These are clearly evidenced the successful synthesis of N-CNT/Fe_3O_4 Cs.

Furthermore, XPS measurements were performed to study the chemical states of different as-prepared carbon samples. XPS survey scan (Fig. 2a) shows clear C 1s, O 1s, and N 1s signals in PDA-CNT, N-CNT, PDA-CNT/Fe_3O_4, and N-CNT/Fe_3O_4 samples and no clear signal for N 1s in CNTs, indicating that the PDA successfully coated the CNT surface via mussel-inspired chemistry and N was successfully introduced into the N-CNT/Fe_3O_4 samples. For details, high-resolution C 1s spectra of N-CNT/Fe_3O_4 samples produced three peaks with binding energies at about 283.4 eV, 284.1 eV, and 285 eV (Fig. 2b). More interestingly, the dominant peak at 283.4 eV corresponds to sp^2 graphitic C atoms(C=C) in CNTs, which is much lower than that of PDA-CNT/Fe_3O_4 (283.7 eV) (Fig. S4c). The similar result was also observed in the C 1s spectra of N-CNT samples (main peak at 283.3 eV) (Fig. S4b) with a lower dominant peak compare with PDA-CNT (284.1 eV) (Fig. S4a) and pristine CNT (284.4 eV) (Fig. S3). The shift of C ls peak toward lower binding energy after dopamine-derived N-Doping by

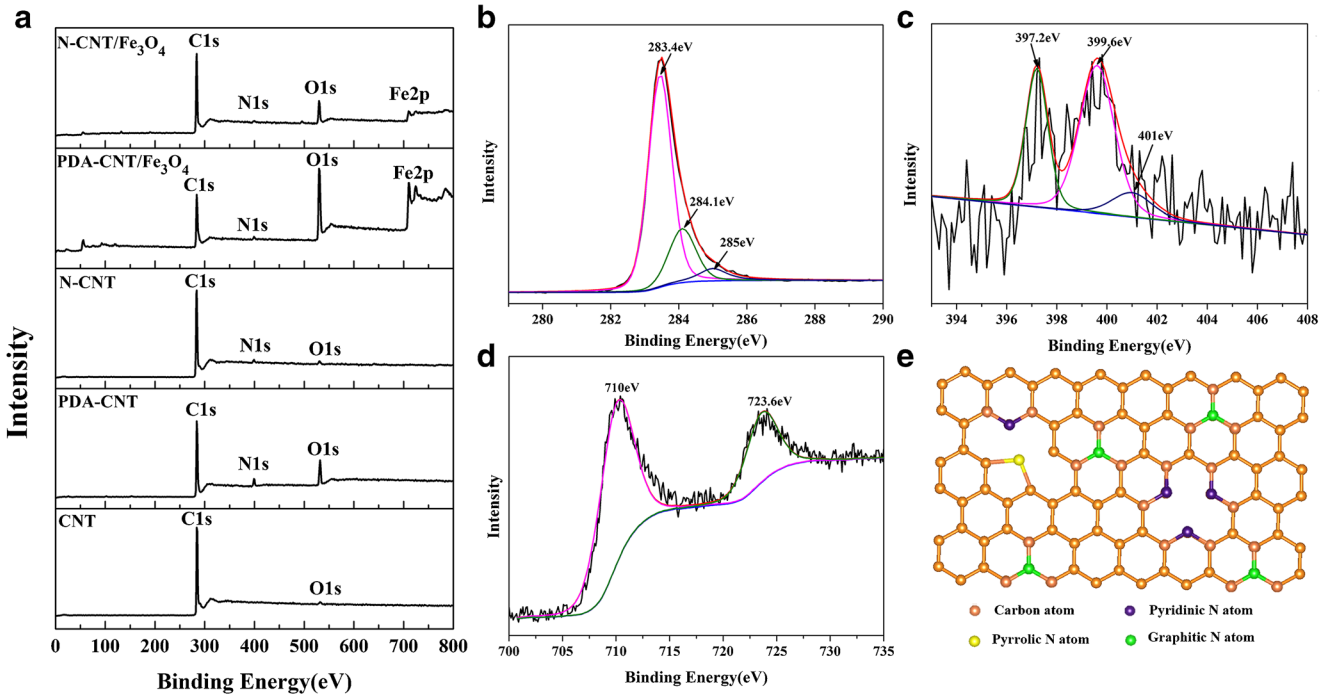

Fig. 2 XPS survey scan of CNT, PDA-CNT, N-CNT, PDA-CNT/Fe_3O_4, and N-CNT/Fe_3O_4 samples (**a**). High-resolution XPS spectra of C1s (**b**), N1s (**c**), and Fe 2p (**d**) in N-CNT/Fe_3O_4 samples. Schematic illustration of pyridinic N, pyrrolic N, and graphitic N in N-doped graphitic structure (**e**)

carbonization indicated that electrons in CNT seem to flow and escape more easily. Meanwhile, the peak at 285 eV of N-CNT/Fe_3O_4 (Fig. 2b) and the peak at 285.1 eV of N-CNT (Fig. S4b) belong to sp^3-bonded carbon with oxygen (C-O) and nitrogen (C-N) [28]. Remarkably, the samples of PDA-CNT/Fe_3O_4 and PDA-CNT exhibit C 1s peak at 287.8 eV and 287.5 eV respectively due to the existence of C=O on its surface [29](Fig. S4a and c), while the peak was disappeared after carbonization in N-CNT/Fe_3O_4 and N-CNT samples (Fig. 2b and S4b).

Another important feature as illustrated in Fig. 2c, N 1s spectra of N-CNT/Fe_3O_4 samples contained three peaks with binding energy located at about 397.2 eV, 399.6 eV, and 401 eV, which correspond to pyridinic N, pyrrolic N, and graphitic N, respectively. As shown in Fig. 2e, pyridinic N originate from sp^2 hybridized N atoms with two sp^2 hybridized C neighbors and pyrrolic N is incorporated in five-membered heterocyclic ring, of these two groups can contribute one or two p-electrons to the π-conjugated system in the graphene layers [28, 30]. The peak of graphitic N suggests that sp^2 hybridized N substituted carbon atoms are incorporated into the graphene layer [31]. While only one obvious N1s peak at 399.4 eV of pyrrolic N can be observed in the sample of PDA-CNT/Fe_3O_4 samples (Fig. S4f). We also found the same results in the N1s spectra of PDA-CNT and N-CNT samples from Fig. S4d and e. These results demonstrate that high-temperature calcination can effectively modulate the chemical state of N in doped CNTs, and pyridinic N and graphitic N may render higher electrical conductivity that is benefit for electrochemical activity of the carbon materials. The XPS of C 1s and N 1s spectra indicated the cross-link of PDA on the surface of CNTs during carbonization, while N atoms are also present in the cross-linked structure [16]. The high-resolution Fe2p spectrum of N-CNT/Fe_3O_4 samples is shown in Fig. 2d. The main peaks at 710 and 723.6 eV are typical binding energy peaks of Fe2p3/2 and Fe 2p1/2 states for Fe_3O_4 [32]. These data confirm the successful preparation of N-CNT/Fe_3O_4.

Electrocatalytic reduction of H_2O_2 on N-CNT/Fe_3O_4 Cs modified electrode

The electrocatalytic behavior of N-CNT/Fe_3O_4 Cs toward H_2O_2 was investigated by cyclic voltammetry (CV) in N_2 saturated 0.01 M PBS (pH 7.4) with addition of different concentration of H_2O_2. As shown in Fig. 3a, electrocatalytic reaction in N-CNT/Fe_3O_4 Cs between Fe (II) and Fe (III) species occurred on the surface of this as-prepared electrode with an oxidative peak at − 0.09 V and a reductive peak at 0.34 V, while an obvious reduction current with peak potential at − 0.65 V is observed after addition of H_2O_2, and the current is enhanced with the increased H_2O_2 concentration. To compare the electrocatalytic behaviors of different modified electrodes to H_2O_2 reduction including Fe_3O_4@GCE, CNT/Fe_3O_4@GCE, PDA-CNT/Fe_3O_4@GCE, and N-CNT/Fe_3O_4@GCE, CV was performed in the present of 2 mM H_2O_2. It can be seen in Fig. 3b that the H_2O_2 sensors fabricated by of Fe_3O_4@GCE, CNT/Fe_3O_4@GCE, PDA-CNT/

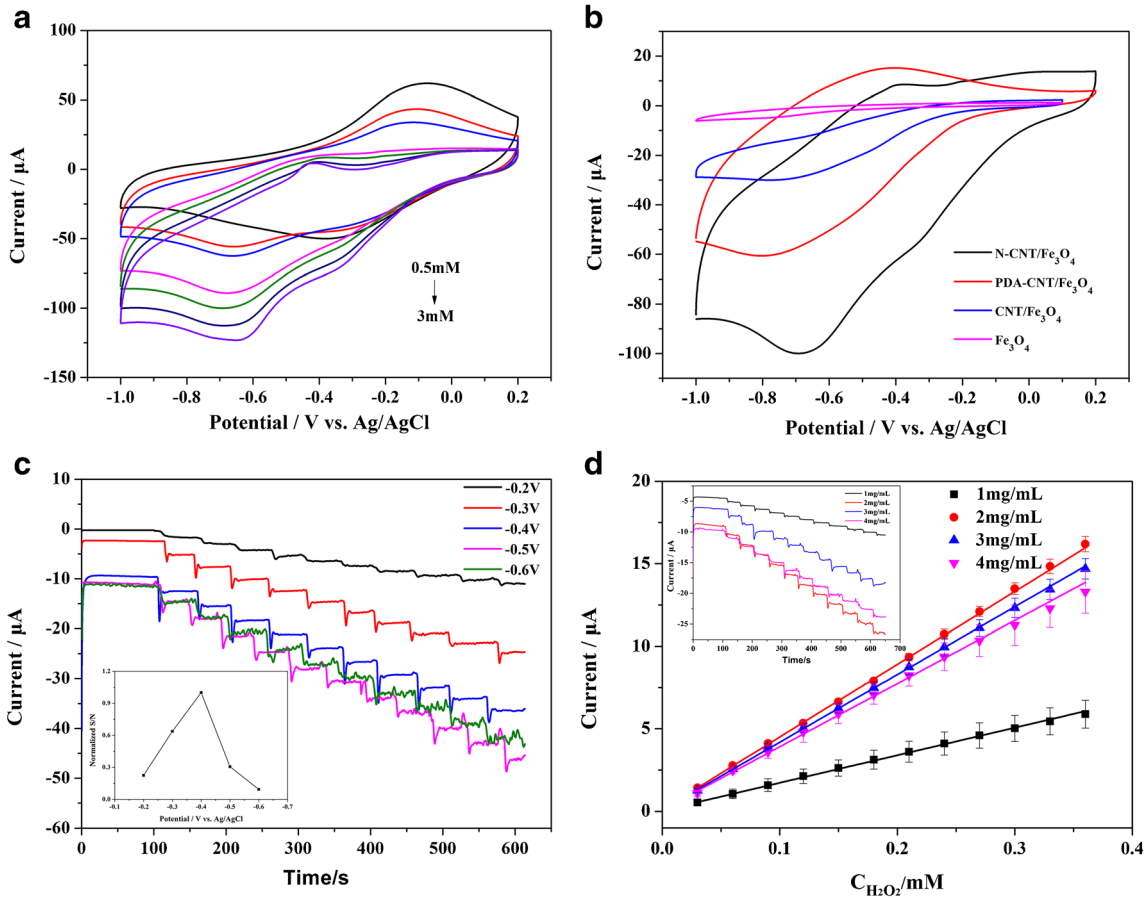

Fig. 3 **a** CVs of N-CNT/Fe_3O_4@GCE in presence of different concentrations of H_2O_2 in N_2 saturated 0.01 M pH 7.4 PBS solution at a scan rate of 50 mV s^{-1}; **b** CV curves of N-CNT/Fe_3O_4@GCE, PDA-CNT/Fe_3O_4@GCE, CNT/Fe_3O_4@GCE, and Fe_3O_4@GCE in the presence of 2 mM H_2O_2. **c** Optimization study of the applied potential employed of N-CNT/Fe_3O_4@GCE. Inset: Plot of the signal-to-noise ratio the applied potential; **d** The PDA-CNTs feedstock concentration for hybrid synthesis in range from 1 to 4 mg/mL. Inset: I-t curves of N-CNT/Fe_3O_4@GCE with the successive addition of 30 μM H_2O_2

Fe_3O_4@GCE, and N-CNT/Fe_3O_4@GCE produce H_2O_2 reduction peak potentials at 0.78 V(pink line), 0.75 V(blue line), 0.79 V(red line), and 0.65 V(black line) respectively. N-CNT/Fe_3O_4@GCE has more positive reduction peak potential, higher electrocatalytic peak current, and the improved onset potential (around 0.00 V) than that of other modified electrodes, indicating that N-CNT/Fe_3O_4@GCE possesses the highest electrocatalytic activity for the H_2O_2 reduction. Such improved electrocatalytic activity is closely related to the N doping in the CNTs' structure. Pyridinic N could greatly improve the onset potential and graphitic N species could increase the limiting current density. In addition, as expected, PDA-directed Fe_3O_4 nanocrystals uniform distribution on CNTs appeared the homogeneity of the as-prepared nanocomposite, which was believed to play a crucial role for the enhanced electrochemical performance. The reaction kinetic process of H_2O_2 electroreduction on modified electrode is diffusion-controlled process. The data and the texts are given in ESM (Fig. S5).

Amperometric response to H_2O_2 detection

To characterize the sensing performance of the N-CNT/Fe_3O_4 electrode toward H_2O_2 detection, time-based amperometric measurement was further performed with the successive addition of 30 μM H_2O_2 into the stirred N_2 saturated 0.01 M PBS. However, the applied potential usually has a large influence on the sensitivity. It is noted that the reduction currents are significantly increased by continuously adding 30 μM H_2O_2 under different applied potentials, as shown in Fig. 3c, but susceptibility to other substances under high negative potential results the higher signal-to-noise ratio on the current response signal [33]. The plot of signal-to-noise ratio versus applied potential in inset of Fig. 3c shows that − 0.4 V is the optimal one for the following experiments. Meanwhile, the loading capacity of Fe_3O_4 in the hybrid material has a significant impact on the sensitivity of H_2O_2 detection. As shown in Fig. 3d, in the range from 1 to 4 mg/mL of feedstock concentration of the PDA-CNTs in synthesis process, the sensitivity

increased and reached the maximum at the concentration of 2 mg/mL, and then the corresponding Fe_3O_4 content in this hybrid is determined by TGA analysis that was about 84.74 wt% (Fig. S6). Therefore, applied potential of − 0.4 V and 2 mg/mL PDA-CNTs feedstock concentration for hybrid synthesis were employed in this study.

The typical current-time (i-t) curves of N-CNT/Fe_3O_4 electrode were further investigated under optimal conditions with the successive addition of varying concentrations H_2O_2. A stepwise current response was observed with increasing H_2O_2 concentration at applied potential of − 0.4 V (Fig. 4a), quickly reaching steady state within 4 s. The calibration curves of the response currents were linear in the concentration ranges of 0.006–2.057 mM with a correlation coefficient of $R^2 = 0.990$ (Fig. 4b). The linear equation is $I\,(\mu A) = 44.12\ C_{H2O2}\ (mM) + 0.1973$ with a detection limit of 0.304 μM at the S/N ratio of 3. The detection sensitivity of N-CNT/Fe_3O_4@GCE was calculated to be 316.27 mA M^{-1} cm^{-2}. The N-CNT/Fe_3O_4@GCE is

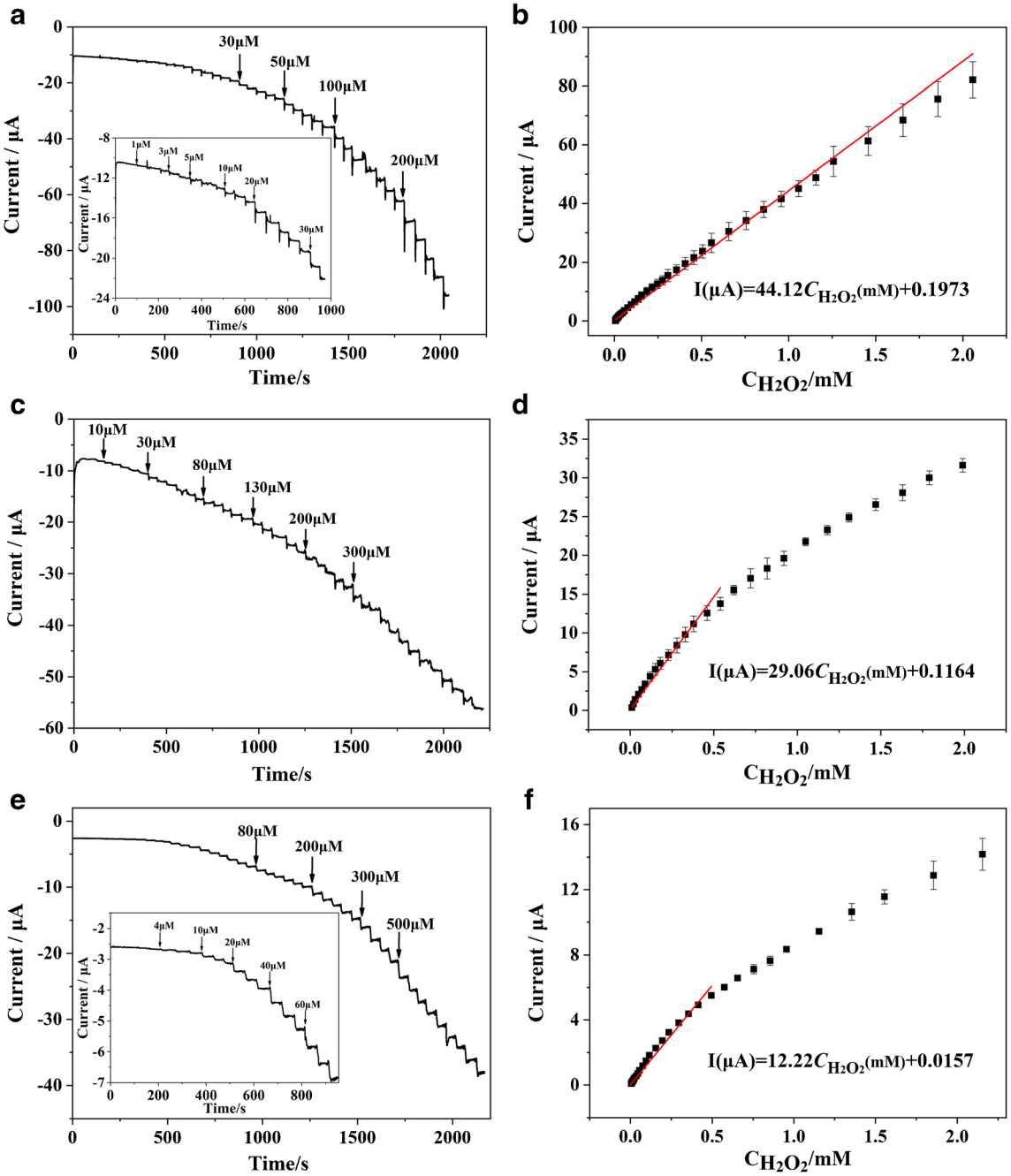

Fig. 4 Amperometric response of N-CNT/Fe_3O_4@GCE (**a**), PDA-CNT/Fe_3O_4@GCE (**c**), and bulk N-CNT/Fe_3O_4@GCE (**e**) to successive additions of H_2O_2 at − 0.4 V in the stirred N_2 saturated 0.01 M pH 7.4 PBS. Calibration curves of N-CNT/Fe_3O_4@GCE (**b**), PDA-CNT/Fe_3O_4@GCE (**d**), and bulk N-CNT/Fe_3O_4@GCE (**f**) between the amperometric response and H_2O_2 concentration

comparable with that reported previously based on advanced catalysts or enzymes biosensors (Table S1). The detection sensitivity of PDA-CNT/Fe_3O_4@GCE and bulk-N-CNT/Fe_3O_4@GCE were also investigated. There are also an obvious reduction current in the CV of PDA-CNT/Fe_3O_4@GCE and bulk-N-CNT/Fe_3O_4@GCE after addition of H_2O_2, accompanying with an enhanced current with the increased H_2O_2 concentration (Fig. S8). As shown in Fig. 4c and d, the PDA-CNT/Fe_3O_4@GCE has a linear relationship with the H_2O_2 concentration in the range of 0.01–0.54 mM. The linear equation was I (μA) = 29.06 C_{H2O2} (mM) + 0.1164 with a sensitivity of 222.51 mA M^{-1} cm^{-2}. The detection limit is 1.2 μM. In Fig. 4e and f, the linear equation for bulk-N-CNT/Fe_3O_4@GCE was I (μA) = 12.22 C_{H2O2} (mM) + 0.0157 with the relevant linear range of 0.004–0.495 mM, and the sensitivity was calculated to be 132.25 mA M^{-1} cm^{-2}. The detection limit is 0.948 μM. These results indicate that N-CNT/Fe_3O_4@GCE reveals the highest sensitivity and a wider linear range compared to PDA-CNT/Fe_3O_4@GCE and bulk-N-CNT/Fe_3O_4@GCE, and further suggest that the synthesis process of phosphate treatment and carbonization can bring about the enlarged electroactive surface area (Fig. S7) and an enhanced sensitivity for H_2O_2 amperometric sensing.

The selectivity of N-CNT/Fe_3O_4@GCE for H_2O_2 reduction was carried out with some possible electroactive compounds in biological system including amino acid (Glutataione (GSH), Cystine (Cys) Tryptophan (Trp)), ions (O_2^- and NO^{3-}) and some biomolecule (nitric oxide (NO), uric acid (UA), ascorbic acid (AA), and dopamine (DA). Figure 5a displays that the modified electrode has no obvious current response to these interfering species with the concentration of 1 mM, and there was a remarkably current response to the addition of 30 μM H_2O_2. This verified that the sensor possesses excellent selectivity for electrochemical detection of H_2O_2.

Reproducibility and storage stability are another crucial factors to develop a promising biosensor. The device-to-device reproducibility was evaluated on the basis of five independently N-CNT/Fe_3O_4@GCE, as shown in Fig. 5b, which demonstrate good reproductivity with a relative

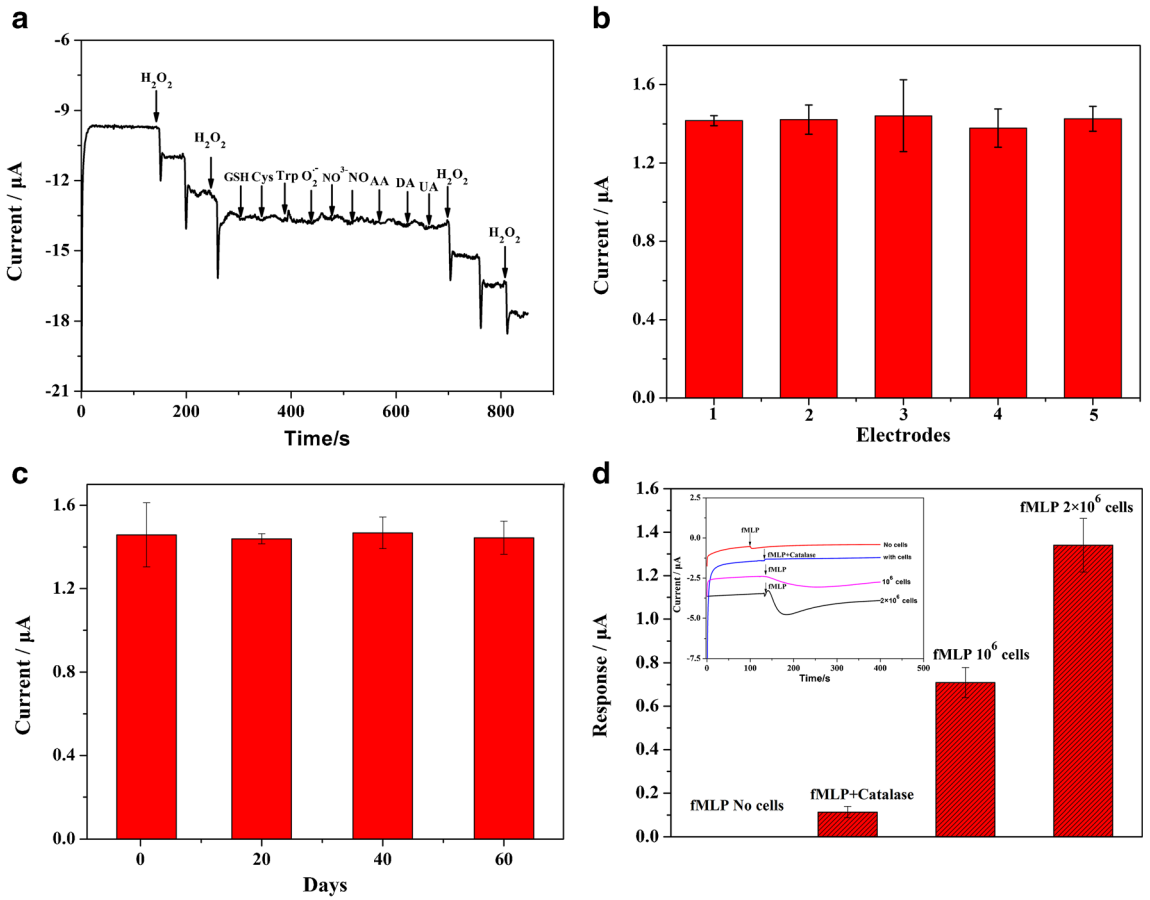

Fig. 5 **a** Amperometric response to successive addition of 30 μM H_2O_2 and 1.0 mM other interferences at applied potential of − 0.4 V; The reproducibility (**b**) and stability test (**c**) of the N-CNT/Fe_3O_4@GCE in 30 μM H_2O_2 in 0.01 M PBS solution. **d** Corresponding plots of amperometric response to fMLP stimulation. Inset: Amperometric response of N-CNT/Fe_3O_4@GCE to the addition of fMLP stimulation with and without EC-9 cells at applied potential of − 0.4 V

standard deviation of 2.0% (RSD) for the H_2O_2 sensitivity. After storage at room temperature for 2 months, the catalytic activity could retain more than 98% of the original current responses toward 30 μM H_2O_2, indicating that the fabricated N-CNT/Fe_3O_4@GCE had excellent storage stability (Fig. 5c).

Real-time detection of H_2O_2 released from living cells

The applicability of the N-CNT/Fe_3O_4@GCE for in situ detection toward cell-released H_2O_2 was further evaluated. As one of important byproducts and an essential mediator in redox modifications of cell biology and pathology, H_2O_2 plays an important role in signaling transduction, cell proliferation, cell apoptosis, and disease occurrence. The amperometric technique exhibits the advantage of real-time monitoring for the dynamic release process of H_2O_2 from living cells, which is of great significance for us to understand its biological effects. The amperometric current response of N-CNT/Fe_3O_4@GCE was recorded at a constant potential of − 0.4 V in 0.01 M PBS (pH 7.4) solution with and without cells. As shown in Fig. 5d, the sensor in the EC-109 cells suspension shows an obvious current change after injecting 4 μM fMLP, and the maximum current responses caused by the number of 2×10^6 cells corresponding about 1.34 μA were about1.9 times than 10^6 cells that of 0.709 μA. For comparison, there were negligible current response in control groups under fMLP stimulation without cells and the addition of 200 μg mL^{-1} catalase selective scavenging of H_2O_2 with cells, suggesting that the response resulted from cell-released H_2O_2 under the stimulation of the drug. These results suggest that N-CNT/Fe_3O_4Cs can be used as high-performance catalysts and biomimetic enzyme for potential applications in bioanalysis and pathological studies.

Conclusion

The synergistic integration of nitrogen-doped carbon with various functional materials is a promising approach to modulate the outstanding material properties of carbon composite for electrocatalytic application. In this approach, a feature structure, dopamine-derived N-doped carbon nanotubes/Fe_3O_4 composites was designed via facile hydrothermal route and calcination treatment. Dopamine as N-containing precursors can offer at least three merits: (1) Dopamine can be self-polymerized on the surface of CNTs that improved the dispersion of CNTs; (2) the unique molecular structure of PDA can promote Fe_3O_4 nanocrystals deposition uniformly on the surface of CNTs; (3) Carbonized polydopamine coatings effectively modulated the graphitic structure and the increased pyridinic N and graphitic N further improved electrochemical performance of carbon composites. Electrochemical measurement results show that the N-CNT/Fe_3O_4@GCE displayed the enhanced electrocatalytic activity for H_2O_2 sensing compared with the PDA-CNT/Fe_3O_4@GCE and the bulk-N-CNTs/Fe_3O_4@GCE. This facile and effective method will open up a new avenue for the development of high-performance electrocatalytic materials for biosensenor and catalytic applications. The proposed N-CNT/Fe_3O_4@GCE sensor demonstrates excellent ability to monitor H_2O_2 released from living cells, which is significant in the application for clinical diagnostics and pathological investigations.

Funding This work was supported by the National Natural Science Foundation of China (81772290), Graduate Scientific Research and Innovation Foundation of Chongqing, China (Grant No. CYB19041), Fundamental Research Funds for the Central Universities (2019CDYGZD007, 2020CDCGSW052), Strong-flavor Baijiu Solid-state Fermentation Key Laboratory of China light industry (2019JJ002), Fundamental Research Funds for the Central Universities (SWU119050), Chongqing science and technology commission (CSTC2018jcyjAX0062), Chongqing Graduate Tutor Team Construction Project, Analytical and Testing Center of Chongqing University (XPS and XRD), and sharing fund of Chongqing University's large equipment.

Compliance with ethical standards

Conflict of interest The authors declare that they have no competing interests.

References

1. Kim ID, Choi SJ, Cho HJ (2015) Graphene-based composite materials for chemical sensor application. 96:65–101
2. Borenstein A, Hanna O, Ran A, Luski S, Brousse T, Aurbach D (2017) Carbon-based composite materials for supercapacitor electrodes: a review. J Mater Chem A 5(25):12653–12672
3. Liu X, Dai L (2016) Carbon-based metal-free catalysts. Nat Rev Mater 1:16064
4. Shin Y-R, Jeon I-Y, Baek J-B (2012) Stability of multi-walled carbon nanotubes in commonly used acidic media. Carbon 50(4):1465–1476
5. Guo CX, Shen YQ, Dong ZL, Chen XD, Lou XW, Li CM (2012) DNA-directed growth of $FePO_4$ nanostructures on carbon nanotubes to achieve nearly 100% theoretical capacity for lithium-ion batteries. Energy Environ Sci 5(5):6919–6922
6. Zhang S, Shao T, Kose HS, Karanfil T (2012) Adsorption kinetics of aromatic compounds on carbon nanotubes and activated carbons. Environ Toxicol Chem 31(1):79–85
7. Sun Y-P, Fu K, Lin Y, Huang W (2002) Functionalized carbon nanotubes: properties and applications. Acc Chem Res 35(12): 1096–1104
8. Wang Y, Wu J, Wei F (2003) A treatment method to give separated multi-walled carbon nanotubes with high purity, high crystallization and a large aspect ratio. Carbon 41(15):2939–2948
9. Lee WJ, Maiti UN, Lee JM, Lim J, Han TH, Kim SO (2014) Nitrogen-doped carbon nanotubes and graphene composite structures for energy and catalytic applications. Chem Commun 45(30): 6818–6830
10. Muhulet A, Miculescu F, Voicu SI, Schütt F, Thakur VK, Mishra YK (2018) Fundamentals and scopes of doped carbon nanotubes towards energy and biosensing applications. Mater Today Energy 9:154–186

11. Haq AU, Lim J, Yun JM, Lee WJ, Han TH, Kim SO (2013) Direct growth of polyaniline chains from N-doped sites of carbon nanotubes. Small 9(22):3829–3833
12. Lin Z, Waller G, Liu Y, Liu M, Wong CP (2012) Facile synthesis of nitrogen-doped graphene via pyrolysis of graphene oxide and urea, and its electrocatalytic activity toward the oxygen-reduction reaction. Adv Energy Mater 2(7):884–888
13. Meng Y, Wu P, Wang Y, Fang W, Zhao F, Du J, Zhang P, Tang Y, Wei S, Zhou Y (2016) Polypyrrole-derived nitrogen-doped carbon nanotubes: template-directed synthesis and enhanced sodium-storage performance. J Taiwan Inst Chem Eng 65:552–557
14. Lai L, Potts JR, Zhan D, Wang L, Poh CK, Tang C, Gong H, Shen Z, Lin J, Ruoff RS (2012) Exploration of the active center structure of nitrogen-doped graphene-based catalysts for oxygen reduction reaction. Energy Environ Sci 5(7):7936–7942
15. Lynge ME, Van der Westen R, Postma A, Städler B (2011) Polydopamine—a nature-inspired polymer coating for biomedical science. Nanoscale 3(12):4916–4928
16. Kong J, Yee WA, Yang L, Wei Y, Phua SL, Ong HG, Ang JM, Li X, Lu X (2012) Highly electrically conductive layered carbon derived from polydopamine and its functions in SnO_2-based lithium ion battery anodes. Chem Commun 48(83):10316–10318
17. Yang L, Wu AY, Si LP, Kong J, Ding H, Cheah JW, Lu X (2012) A high throughput method for preparation of highly conductive functionalized graphene and conductive polymer nanocomposites. RSC Adv 2(6):2208–2210
18. Ai K, Liu Y, Ruan C, Lu L, Lu G (2013) Sp^2 C-dominant N-doped carbon sub-micrometer spheres with a tunable size: a versatile platform for highly efficient oxygen-reduction catalysts. Adv Mater 25(7):998–1003
19. Shen H, Long Y, Yang X, Zhao N, Xu J (2015) Facile fabrication of metal oxide hollow spheres using polydopamine nanoparticles as active templates. Polym Int 64(8):986–991
20. Yan J, Yang L, Lin M-F, Ma J, Lu X, Lee PS (2013) Polydopamine spheres as active templates for convenient synthesis of various nanostructures. Small 9(4):596–603
21. Liu Y, Ai K, Lu L (2014) Polydopamine and its derivative materials: synthesis and promising applications in energy, environmental, and biomedical fields. Chem Rev 114(9):5057–5115
22. Trachootham D, Alexandre J, Huang P (2009) Targeting cancer cells by ROS-mediated mechanisms: a radical therapeutic approach? Nat Rev Drug Discov 8(7):579–591
23. Ma B, Kong C, Hu X, Liu K, Huang Q, Lv J, Lu W, Zhang X, Yang Z, Yang S (2018) A sensitive electrochemical nonenzymatic biosensor for the detection of H_2O_2 released from living cells based on ultrathin concave Ag nanosheets. Biosens Bioelectron 106:29–36
24. Panaro MA, Mitolo V (1999) Cellular responses to Fmlp challenging: a mini-review. Immunopharmacol Immunotoxicol 21(3):397–419
25. Korosi L, Papp S, Meynen V, Cool P, Vansant E, Dekany I (2005) Preparation and characterization of SnO nanoparticles of enhanced thermal stability: the effect of phosphoric acid treatment on SnO·HO. Colloids Surf A Physicochem Eng Asp 268(1–3):147–154
26. Wang C, Li J, Zhang Y, Wei Y, Liu J (2010) The influence of phosphate on crystal grain growth of nanosized SnO_2. J Alloys Compd 493(1):64–69
27. Liu J, Lu B, Liu J, Zhang Y, Wei Y (2011) The hindering function of phosphate on the grain growth behavior of nanosized zirconia powders calcined at high temperatures. Ceram Int 37(3):843–849
28. Luo Z, Lim S, Tian Z, Shang J, Lai L, Macdonald B, Fu C, Shen Z, Yu T, Lin J (2011) Pyridinic N doped graphene: synthesis, electronic structure, and electrocatalytic property. J Mater Chem 21(22):8038–8044
29. Ren F, Zhai C, Zhu M, Wang C, Wang H, Duan B, Guo J, Yang P, Du Y (2015) Facile synthesis of PtAu nanoparticles supported on polydopamine reduced and modified graphene oxide as a highly active catalyst for methanol oxidation. Electrochim Acta 153(2):175–183
30. Wei D, Liu Y, Wang Y, Zhang H, Huang L, Yu G (2009) Synthesis of N-doped graphene by chemical vapor deposition and its electrical properties. Nano Lett 9(5):1752–1758
31. Qu K, Zheng Y, Dai S, Qiao SZ (2015) Polydopamine–graphene oxide derived mesoporous carbon nanosheets for enhanced oxygen reduction. Nanoscale 7(29):12598–12605
32. Li X, Si Z, Lei Y, Tang J, Wang S, Su S, Song S, Zhao L, Zhang H (2010) Direct hydrothermal synthesis of single-crystalline triangular Fe_3O_4 nanoprisms. Crystengcomm 12(7):2060–2063
33. Wang T, Zhu H, Zhuo J, Zhu Z, Papakonstantinou P, Lubarsky G, Lin J, Li M (2013) Biosensor based on ultrasmall MoS_2 nanoparticles for electrochemical detection of H_2O_2 released by cells at the nanomolar level. Anal Chem 85(21):10289–10295